JMEPEG (2011) 20:646–652
DOI: 10.1007/s11665-011-9841-3

1059-9495/$19.00

FE Analysis of Nitinol Leaf Springs Used in a Compression Anastomosis Device

Amir Weizman, Leonid Monassevitch, Kobby Greenberg, Shahar Millis, Boaz Harari, and Idan Dar

(Submitted June 20, 2010; in revised form December 9, 2010)

Reconstruction of the digestive system lumen patency (anastomosis creation) after its partial surgical removal is a common and crucial procedure. The conventional anastomosis methods use devices for mechanical suturing which are associated with high failure risk and can lead to major complications. The compression anastomosis as a sutureless method seems to be a promising alternative. However, attempts during the last two centuries have not been completely successful due to the complex character of the tissue-healing process. The specific mechanical behavior of Nitinol alloys was applied to the force element of the compression devices. These devices are becoming more widely adopted in surgery practice. The compression anastomosis device enables the anastomosis of colonic and intestinal tissue based on compression forces exerted by Nitinol leaf springs. By means of changing the strain distribution in the stressed leaves with varying moments of inertia, one can gain full control of the different stages in the force-deflection profile (i.e., linear elastic stage and the force plateau stage). The target of this study is the comparison of different Nitinol leaf geometries and evaluation of the finite elements analysis as a tool for preliminary design of such geometries. The results of this analysis allow us to establish regulation of the spring's mechanical behavior, thus controlling the anastomosis creation in the compression anastomosis device.

Keywords compression anastomosis, finite elements, leaf springs, Nitinol

1. Introduction

1.1 Compression Anastomosis

Anastomosis is the surgical restoration of the continuity of separated parts of hollow organs. Today, the overwhelming majority of surgeons create anastomosis in the digestive system using surgical staplers which perform uniform mechanical suture. Regardless of the fact that mechanical suturing is still the "gold standard," it suffers from several inherent imperfections. Therefore, the surgical community continues to look forward to finding an appropriate sutureless method.

Compression anastomosis is one of the most promising among sutureless methods; however, attempts during the last two centuries have not been completely successful due to the complex character of the tissue-healing process (Ref 1, 2). The specific mechanical behavior of Nitinol alloys was applied to the force element of compression devices. These devices are becoming widely adopted in surgical practice (Ref 3, 4). The BowelRing™ compression anastomosis element (Fig. 1) enables the anastomosis of intestinal tissue based on compression forces exerted by two Nitinol leaf springs, being superelastic at body temperature. The BowelRing™ consists of an implant in the form of two elliptic plastic rings compressed one against the other by two Nitinol leaf springs. The two rings are connected by stainless steel spikes; these spikes are connected to a steel sheet which is pressed against the Nitinol springs so that detachment of the rings (due to accommodation of tissue) will activate compression forces as a consequence of the deformation of the springs (Fig. 2).

When placed in the anastomotic area, the device is open, and can accommodate varying thicknesses of tissue. The Nitinol leaf springs begin the process of returning to their original shape, and the opening in the device gradually closes. As the compression progresses, the tissue trapped within the ring becomes necrotic, while healthy tissue is generated along the ring's outer perimeter. The ring is released only after the tissue has moved through the phases of healing and gained its full strength.

1.2 Anastomosis Creation

The anastomosis creation process under compression can be divided into three main stages. In the first stage, an applied force must ensure leak tightness and hemostasis in the compressed tissue. As the healing process continues and the tissue thickness is reduced, a slowly decreasing force should be applied irrespective of tissue thickness to prevent leakage.

During the second stage, the biological strength of the anastomosis develops slowly but is still not sufficiently high; hence, the anastomosis integrity is still mainly dependent upon the mechanical strength of the compression ring.

During the last stage of the anastomosis creation (when the trapped tissue becomes thin), the force should significantly drop

This article is an invited paper selected from presentations at Shape Memory and Superelastic Technologies 2010, held May 16-20, 2010, in Pacific Grove, California, and has been expanded from the original presentation.

Amir Weizman, Leonid Monassevitch, Kobby Greenberg, Shahar Millis, and **Boaz Harari**, NiTi Surgical Solutions, Yad Harutzim Street, See'im Industrial Park Building 9E, P.O. Box 8634, 42506 Netanya, Israel; and **Idan Dar**, C.A.S. Ltd., 2 Etgar Street, 39032 Tirat Hacarmel, Israel. Contact e-mails: amir@nitisurgical.com and idan@cas.co.il.

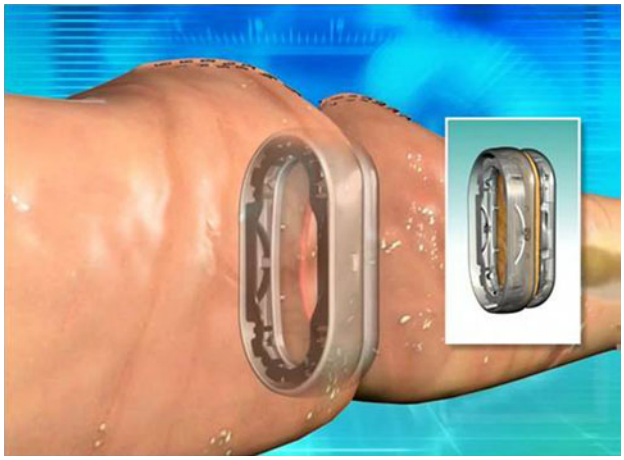

Fig. 1 BowelRing™ anastomosis device (investigational device)

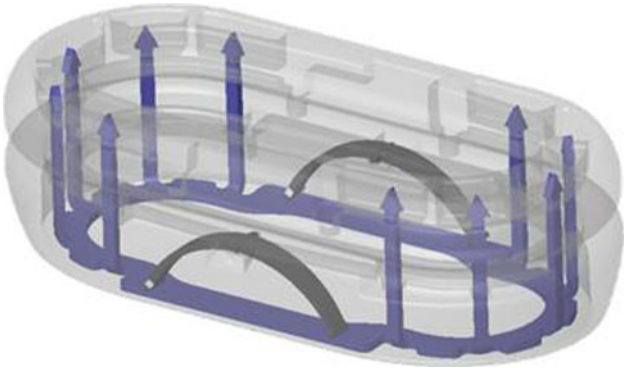

Fig. 2 Nitinol springs assembled within the BowelRing™ device

to slow down the rate of decrease in thickness and to prevent untimely cutting of the thin tissue. A remaining force must ensure the mechanical strength of the anastomosis until biological solidity increases adequately.

Figure 3 presents the typical force profile of the BowelRing™ compression device. The tissue thickness decreases during the healing process, and therefore, the compression profile lies on the unloading curve. As can easily be seen, the nonlinear force profile of the Nitinol springs satisfies all of the above requirements and therefore provides a significant advantage when using it in the process of anastomosis creation. The maximal opening of the compression device is 2.5 mm; hence, the force of the leaf springs should be sufficiently high to compress the tissue to 2.5 mm or less.

While the mechanical behavior of Nitinol is determined by material thermo-mechanical history, the behavior of a specific force element also depends on its geometrical form. By means of changing the strain distribution in the deformed leaves, one can gain full control of the different stages in the force-displacement profile (i.e., linear elastic stage and the force plateau stage). The aim of this study is the comparison of different Nitinol leaf geometries and the evaluation of the finite elements analysis (FEA) as a tool for preliminary design of such geometries. The results of the analysis studies will allow us to establish regulation of the spring's mechanical behavior, thus gaining better control of the anastomosis creation in the compression anastomosis device.

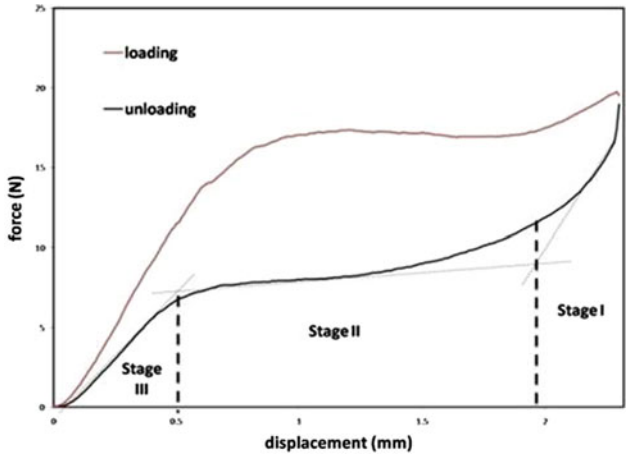

Fig. 3 Typical force profile of the BowelRing™ compression device

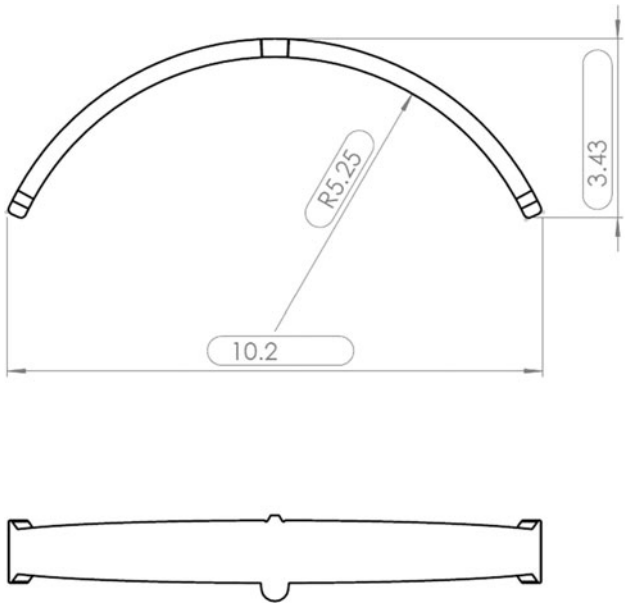

Fig. 4 Dimensions of the leaf springs used in the BowelRing™ device (all dimensions are in mm)

2. Experimental

2.1 Shape Setting and Mechanical Testing

The leaf springs were laser cut from a 0.35 mm, 50.8 at.% Ni Nitinol sheet and shape set at temperatures above 500 °C to form the leaf shape as shown in Fig. 4.

The springs were also aged at 430-480 °C followed by water quenching to obtain a final Af temperature of 15 ± 5 °C.

The Af temperature was measured by the BFR (Bend and Free Recovery) method according to ASTM F2082-06 (Ref 5). In order to control the force profile, additional designs denoted as designs *a*, *b*, and *c* were laser cut as shown in Fig. 5 and 6. These springs were heat treated in the same manner. The force profiles of the springs were evaluated by assembling the springs in the compression device (Fig. 2) and testing for compression forces in a special fixture using a Tinius Olsen H5KT benchtop

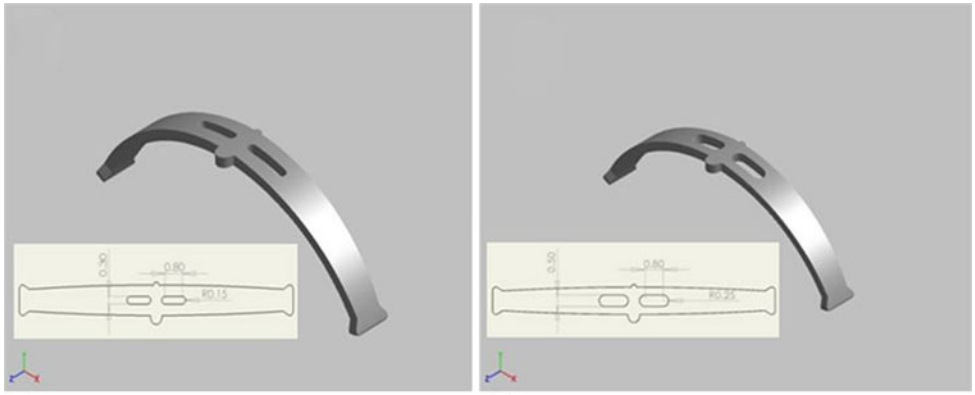

Fig. 5 Leaf design (a) narrow window (b) wide window

Fig. 6 Illustration of design *c*

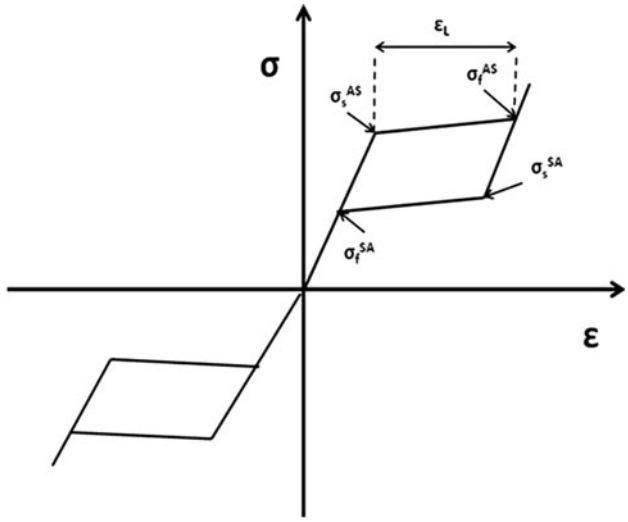

Fig. 7 Material constants according to the ANSYS shape memory alloy material model

testing machine with a 100 N load-cell under temperature-controlled environment at 37 °C.

2.2 Mathematical Modeling

In order to describe the superelastic behavior of the Nitinol springs, the ANSYS shape memory alloy material model was used (Ref 6). This model is based on Aurichio et al. (Ref 7), which treated the superelastic stress-strain profile as four adjoining linear moduli (Fig. 7).

In order to use this model, the following material constants must be input:

- σ_s^{AS}, the starting stress value of the forward austenite to martensite transformation
- σ_f^{AS}, the final stress value of the forward austenite to martensite transformation
- σ_s^{SA}, the starting stress value of the reverse martensite to austenite transformation
- σ_f^{SA}, the final stress value of the reverse martensite to austenite transformation
- ε_L, the maximum super elastic strain
- α, a parameter used in order to evaluate the tension-compression asymmetry
- $E_{\text{Austenite}}$, the elastic modulus of the austenite phase
- $E_{\text{Martensite}}$, the elastic modulus of the martensite phase

Owing to difficulties in fabricating tensile specimens which have the same thermo-mechanical history as the Nitinol springs, the material constants of the springs could not be determined experimentally. Different material models were evaluated to determine the most suitable set of material constants (Table 1). Once selected, this set of constants was used for the analysis of all of the spring designs. Owing to minor effect on the force profile in this case, α was taken as zero, and a tension-compression symmetry was assumed.

The Nitinol leaf spring was modeled by supporting the spring base at the middle line and loading the edge of the leaf to the desired point. Total displacement of 2.5 mm was imposed using two rigid analytic surfaces above and below the spring.

Owing to symmetry considerations only a half-leaf was modeled (Fig. 8); the final results were then multiplied by four as each device consists of two leaves. The boundary condition was selected to be no movement of the nodes on the symmetry plane in a perpendicular direction to that surface; 3D hexahedral elements were used for the analysis, and a mesh refinement was carried out. Frictional contact was used on the bottom (spring edges), as a part of the optimization of the material constants. The optimal value of friction coefficient was found to

Table 1 Selected material constants

$E_{Austenite}$	σ_s^{AS}	σ_f^{AS}	$E_{Martensite}$	σ_s^{SA}	σ_f^{SA}	ε_L	α
60 GPa	470 MPa	470 MPa	20 GPa	350 MPa	350 MPa	0.06	0

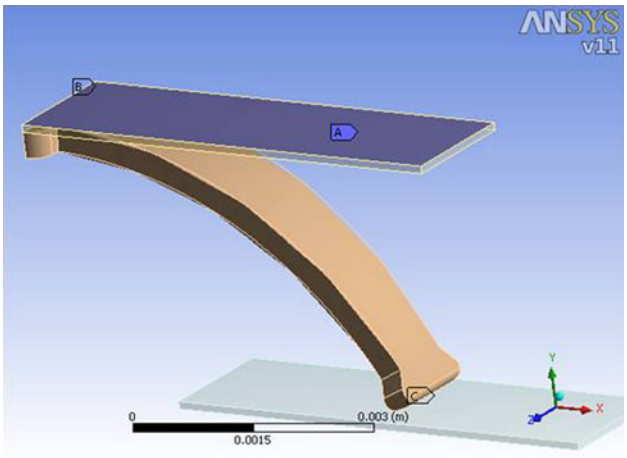

Fig. 8 Modeling of the Nitinol leaf spring

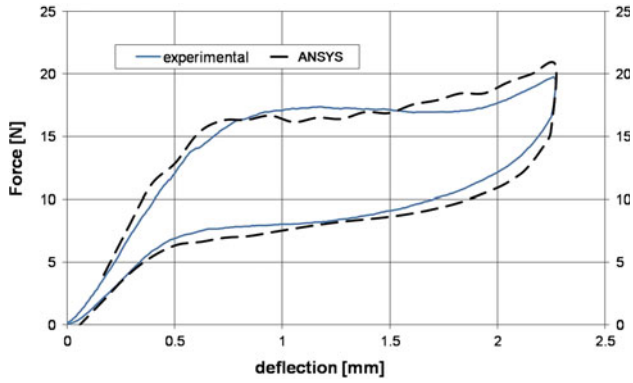

Fig. 9 Experimental vs. calculated force profiles

be 0.3, with a frictionless contact being used on the top (spring base).

3. Results and Discussion

3.1 Basic Design

Figure 9 presents the comparison between the experimental and the calculated force profiles.

When coming to designing the first leaf springs, the maximal strain was estimated by approximating the 2.5-mm deflected deformed shape as a circular arc. Using beam theory (Ref 8), the maximal strain is

$$\varepsilon = \frac{R_o/R - 1}{2R_o/t + 1} = 2.5\% \qquad \text{(Eq 1)}$$

where R_o and R are the radii of the neutral axis before and after deformation, respectively.

Figure 10 presents the FE strains map of the leaf spring deformed to 2.5 mm; according to the FEA, the maximal strain is about 3.3%. Both the beam theory and the FEA indicated that the maximal strain is below the superelastic strain limit (6-8%). This result is backed up by the fact that the leaf showed perfect superelastic force profile with no residual deformation (Fig. 9).

The strain value according to the FE analysis (~3.3%) is higher due to the fact that the deformation of the leaf (Fig. 9) is not uniform. There is localization of the strain near the middle of the leaf where the profile becomes almost flat ($R \to \infty$), whereas the theoretical value assumes uniform distribution. When taking $R \to \infty$ in (1), the maximal strain becomes

$$\varepsilon_{R\to\infty} \approx \frac{t}{2R_o} = 3.2\% \qquad \text{(Eq 2)}$$

This value shows a much better prediction of the maximal strain value as calculated in the FEA, and hence, one can conclude that although Eq 1 cannot be used for the precise prediction of the deformation strains in cases where the deformation profile is not uniform, it can provide a hint for the overall strain and the extreme cases.

The leaf spring has complex strain distribution in which some areas experience superelastic deformation whereas some areas stay in the pure elastic region. The transition from pure elastic to superelastic deformation governs the different stages in the force profiles; hence, the evaluation of different spring geometries will allow us controlling the different stages in the force profile (i.e., linear elastic stage and the force plateau stage).

3.2 New Designs

In order to have better control of the force profile, new designs were tested in which two types of apertures were added to the leaf profile denoted as design *a* and design *b* (Fig. 5).

Figure 11 presents the comparison between the experimental and calculated (FEA) force profiles of the two designs. Although there is some discrepancy at the end of the profiles there is a very good fit between the graphs in both designs. The discrepancy can be attributed to the fact that the addition of the aperture created waviness of the leaf profile which caused the midline to detach from the base in more than 0.1 mm (Fig. 12). In the actual ring, the leaf was threaded through a plastic (HDPE) slot which prevents the leaf from detaching from the base in more than 0.05 mm and caused the sharp increase of force at the end of the edge of the profile. An additional analysis to take this difference into account was not carried out because of our interest had been to focus only on the beginning of the force profile (i.e., stages II and III).

The addition of the apertures leads to lower compression force exerted by the leaves. In order to compensate for this lack of resisting material, the leaves were heat treated to lower the Af temperature from 15 ± 5 to 5 ± 5 °C and as a consequence, increase the unloading plateau force. The Af temperature was

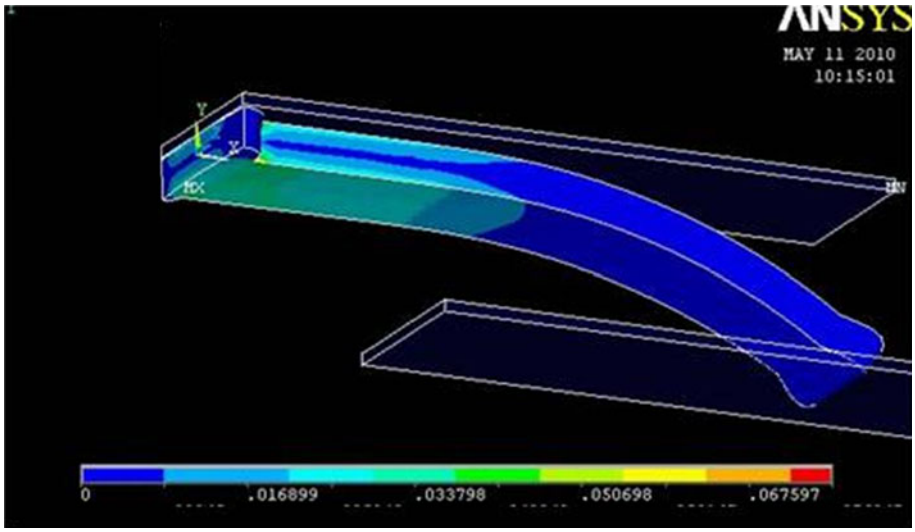

Fig. 10 Strain distribution upon deforming to 2.5 mm

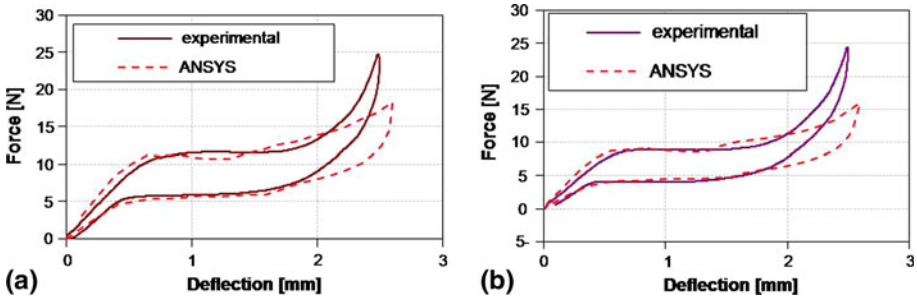

Fig. 11 Unloading force profile (a) narrow aperture (b) wide aperture

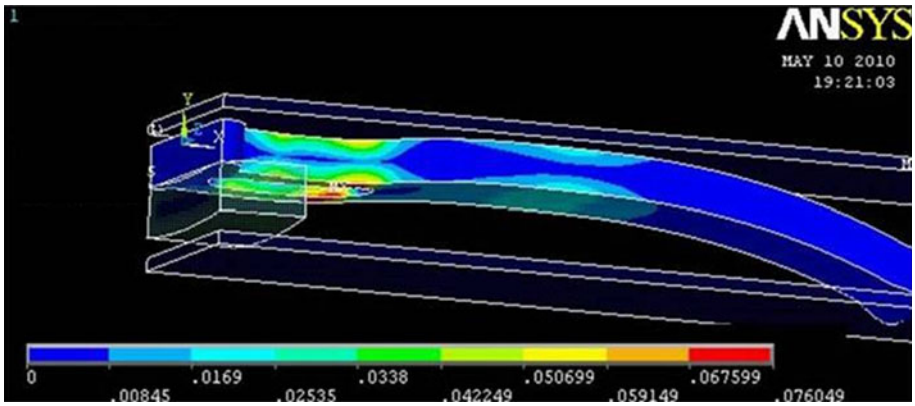

Fig. 12 Deformed profile of design *a*

lowered by heat treating at temperatures above 500 °C for short periods (couple of minutes); too long treatment at this temperature might cause an increase of the Af temperature and an excessive annealing of the alloy (Ref 9).

Figure 13 presents the effect of the Af temperature on the experimental unloading force profile of design *a* (narrow aperture). As one might expect, while the unloading plateau force significantly increases, the slope of the last part of the unloading curve hardly changes upon modifying the Af. This observation is understandable based on the fact that this part corresponds to pure elastic deformation (based on the FEA).

Figure 14 presents the experimental unloading force profiles of designs *a* and *b* in comparison with the original basic full leaf design. The aperture addition significantly flattened the

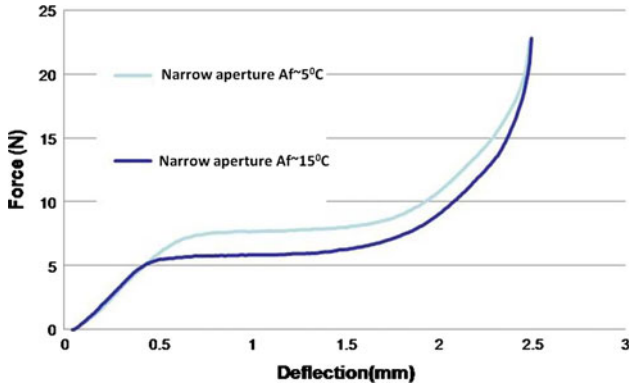

Fig. 13 The effect of the Af temperature on the experimental unloading force profile

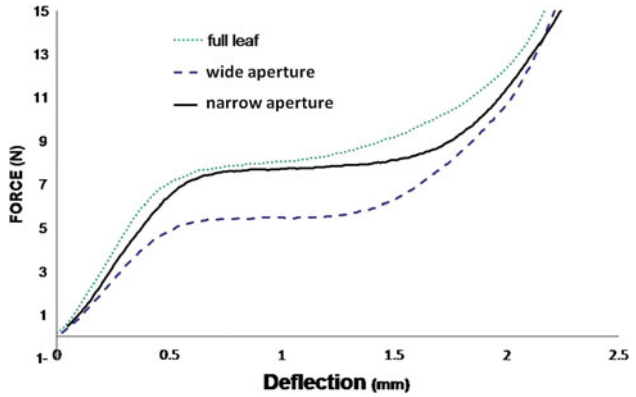

Fig. 14 Experimental unloading force profiles of the different designs

plateau region and decreased the slope of the pure elastic region. The lower slope can be attributed to the fact that in this region the deformation is concentrated only within the aperture region which has lower moment of inertia due to lack of a resisting material. In larger deflection, the maximal strain increases to 6%, localized mainly in the aperture area, which means that higher fraction of the leaf lies within the superelastic region (i.e., transformed to stress-induced martensite). High enough plateau forces could not be achieved in the wide aperture leaf (design *b*) even when treated to achieve lower Af temperature.

Although the aperture's addition to the spring leaf indeed changed the force profile, the control of the different stages is still rather limited, in addition to the fact that the window addition demands a change of the Af temperatures because of the lack of resisting material. In order to better control the different stages of the force profile, an additional design concept was evaluated (Fig. 6). This last design divides the leaf into two parts: peripheral and internal. This design promises a change in the force profile without needing to change the material's properties. Figure 15 presents the comparison between the experimental and calculated (FEA) force profiles of design *c*. There is a fairly good fit between the curves especially in the unloading curve. The fact that the compression of the new design created a two-stage plateau profile is very interesting.

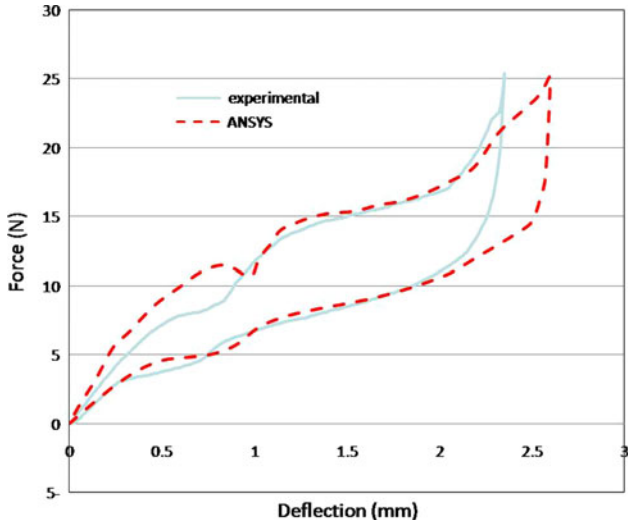

Fig. 15 Unloading force profiles of design *c*, experimental vs. calculated

Observation of the deformation maps at various deflections (Fig. 16) reveals that, in low deflections, only the peripheral part is deformed, and the bending is concentrated on the peripheral material near its division with the inner material. In high deflections, the inner part starts to deform as well, and the bending axis shifts toward the middle of the leaf. This second stage of deformation creates the second plateau in the force deflection curve. When comparing the experimental unloading curve to that of the full leaf (Fig. 17), it can be seen that, in high deflections, the two curves almost overlap because, in this region, the two-stage leaf (design *c*) works almost as a whole unit, and the bending axis lies in the middle of the leaf. On the other hand, in low deformations, design *c* shows the two-stage plateau (marked with the circle), and there is a significant difference between the two curves. The use of the new two-part design creates an additional degree of freedom that enables us to gain better control of the transition from the different stages in the unloading force profile. The improved control possesses immense potential when coming to design compression anastomosis devices as a result of the ability to better control the anastomosis creation under the compression regime.

4. Summary and Conclusions

A rather good fitting between the experimental force profiles and the calculated profiles based on the FE analysis was obtained using the ANSYS shape memory alloy material model. The model proved itself to be an efficient tool for preliminary design of Nitinol force elements. The comparison of the different leaf geometries allows us to gain better control of the different stages of the force profile, including flattening of the plateau force region and even creation of an additional plateau stage. The improved control of the force profile allows us gaining better control of the anastomosis healing process and possesses immense potential when coming to designing compression anastomosis devices.

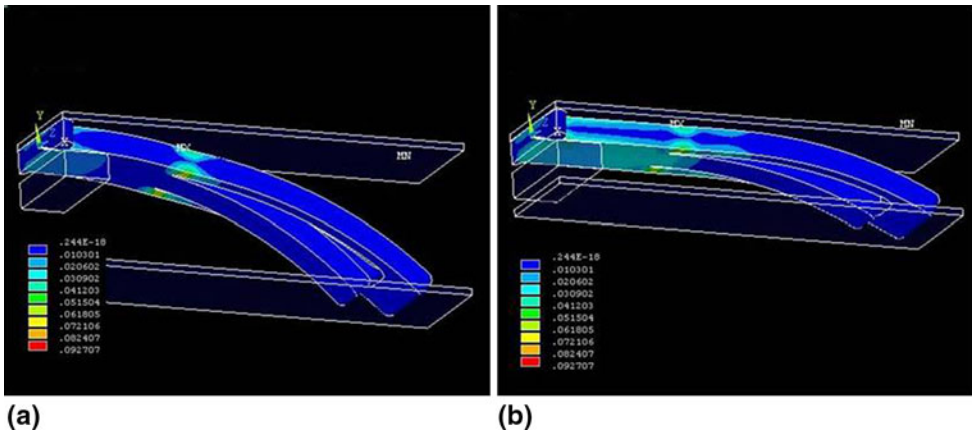

Fig. 16 Deformed profile of design *c* (a) low deflection (b) high deflection

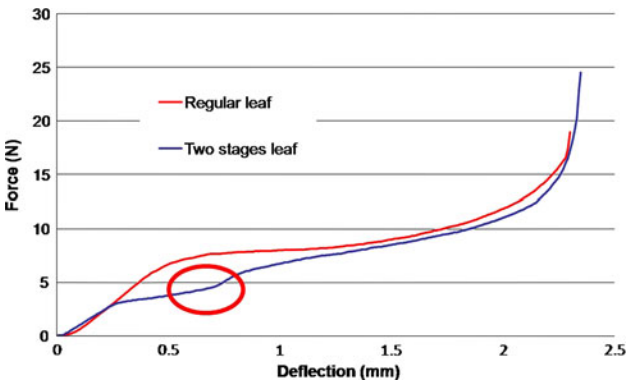

Fig. 17 Experimental unloading profile, design *c* vs. original full leaf design

References

1. R. Aggarwal and A. Darzi, Compression Anastomosis Revisited, *J. Am. Coll. Surg.*, 2005, **201**(6), p 965–971
2. O.K. Person, R.J. Rosenthal, S.D. Wexner, S. Szomstein, and B. Person, Compression Anastomosis: History and Clinical Considerations, *Am. J. Surg.*, 2008, **195**(6), p 818–826
3. L. Monassevitch, N. Bendov-Laks, N. Tyagunov, A. Perle, S. Lelcuk, D. Kopelman, and A. Szold, Design Principles of Shape Memory Devices for Compression Anastomosis in the Digestive System, SMST-2006, *Proceedings of the International Conference on Shape Memory and Superelastic Technologies*, B. Berg, M.R. Mitchell, and J. Proft, Ed., May 7–11, 2006 (Pacific Grove, CA), ASM International, 2006, p 703–713
4. B. Dauser and F. Herbst, NITI, Endoluminal Compression Anastomosis Ring (NITI, CAR 27®): A Breakthrough in Compression Anastomoses?, *Eur. Surg.*, 2009, **41**(3), p 116–119
5. "Standard Test Method for Determination of Transformation Temperature of Nickel-Titanium Shape Memory Alloys by Bend and Free Recovery," F2082, ASTM, p 1–5
6. ANSYS Inc., Programmer's Manual for ANSYS—ANSYS Release 11.0, 2007
7. F. Auricchio, R.L. Taylor, and J. Lubliner, Shape-memory Alloys: Macromodelling and Numerical Simulations of the Superelastic Behavior, *Comput. Method Appl. Mech. Eng.*, 1997, **146**(3–4), p 281–312
8. V.E. Gunter, V.I. Itin, and L. Monassevitch, Effekty Pamiati Formy I ikh Primienenie v Medicinie, Nauka (Novosibirsk, 1992), 742 p (in Russian)
9. D. Favier, Y. Liu, L. Orgéas, A. Sandel, L. Debove, and P. Comte-Gaz, Influence of Thermomechanical Processing on the Superelastic Properties of a Ni-Rich Nitinol Shape Memory Alloy, *Mater. Sci. Eng. A*, 2006, **429**, p 130–136